We are IntechOpen,
the world's leading publisher of Open Access books
Built by scientists, for scientists

6,900
Open access books available

186,000
International authors and editors

200M
Downloads

154
Countries delivered to

Our authors are among the

TOP 1%
most cited scientists

12.2%
Contributors from top 500 universities

BOOK CITATION INDEX
CLARIVATE ANALYTICS
INDEXED

WEB OF SCIENCE™

Selection of our books indexed in the Book Citation Index
in Web of Science™ Core Collection (BKCI)

Interested in publishing with us?
Contact book.department@intechopen.com

Numbers displayed above are based on latest data collected.
For more information visit www.intechopen.com

Chapter

Kinetostatic Nonlinear Stiffness Characteristic Generation Using the Kinematic Singularity of Planar Linkages

Baokun Li and Guangbo Hao

Abstract

The theory of nonlinear stiffness characteristic by employing the kinematic limb-singularity of planar mechanisms with attached springs is proposed. After constructing the position formula with closed-loop form of the mechanism, the kinematic limb-singularity can be identified. The kinetostatic model can be obtained based on the principle of virtual work. The influences of spring stiffness on the force-displacement or torque-angle curve are analysed. Different spring stiffness results in one of four types of stiffness characteristic, which can be used to design an expected stiffness characteristic. After replacing corresponding joints with flexures, the pseudo-rigid-body model of the linkage with springs is obtained. The compliant mechanisms with nonlinear stiffness characteristic can further be synthesised based on the pseudo-rigid-body model.

Keywords: kinematic singularity, nonlinear stiffness, kinetostatic model, planar linkage with springs, compliant mechanism

1. Introduction

A planar linkage always arrives at some several special positions, which may decrease the stability, disable the motion ability or change the degree of freedom of the linkage. These special positions are called kinematic singular configuration or kinematic singularity. It is one of intrinsic properties of the linkage [1].

Kinematic singularity attracted many scholars' attention since it affects the performance of the linkage. Kinematic singularity classification, singularity identification and singularity property, with a particular emphasis on eliminating or avoiding the singularities, are discussed [2–8].

However, everything has two sides. Kinematic singularity of linkages can also be applied to create new useful devices, such as fixture based on the dead-point singularity. In recent years, some compliant mechanisms with new performance are constructed using the kinematic singularity [9–12].

For a generic planar linkage, kinematic limb-singularity and kinematic actuation-singularity may often be exhibited. In this chapter, we mainly introduce how to use the kinematic limb-singularity of the linkage with placing springs at corresponding joints to generate the kinetostatic nonlinear stiffness, which can also

be used to synthesise the nonlinear stiffness compliant mechanisms using the pseudo-rigid-body model (PRBM) [13, 14].

2. Position analysis and kinematic singularity identification

Position analysis is the base of the kinematic singularity determination and singularity classification. Many approaches can be used to carry out the position analysis. Graphical methods often provide a fast and efficient means of analysing mechanisms. Analytical methods are currently more common because of the ease in which they are programmed. Here we mainly use the closed-form solution to present the position analysis of the planar linkage followed by the kinematic singularity identification.

By a generic planar double-slider linkage as an example, the position analysis using the closed-form equation and the kinematic singularity identification are introduced.

Consider a planar double-slider linkage with given structure parameters as shown in **Figure 1**.

The right-hand rule fixed frame O-XYZ is attached on the base, where the intersection point of two paths of points A and B is set as the origin O. We suppose that the moving direction of the input slider is the negative of X-axis. The rotation angle from the negative moving direction of point A to the initial moving direction of point B is defined by α. Line AC is the vertical line from point A to line OB, where point C is the foot. The position vectors of points A and B with respect to the fixed frame O-XYZ are defined by $\boldsymbol{r}_A$ and $\boldsymbol{r}_B$, respectively. The position vector from point A to point B is defined by $\boldsymbol{r}_{AB}$. Thus the closed-loop vector equation of the linkage as shown in **Figure 1** can be obtained as

$$\boldsymbol{r}_A + \boldsymbol{r}_{AB} = \boldsymbol{r}_B \tag{1}$$

The X-axis coordinate of point A is defined by r_A, the rotation angle from vector $\boldsymbol{r}_A$ to vector $\boldsymbol{r}_B$ is defined by θ_A, the distance between point B and origin O is defined by scalar r_B, and the length of the coupler AB is defined by scalar r_{AB}. Thus, based on Eq. (1), two algebraic equations can be transformed as follows:

$$\begin{cases} r_A + r_{AB} \cos\theta_A = r_B \cos\alpha \\ r_{AB} \sin\theta_A = r_B \sin\alpha \end{cases} \tag{2}$$
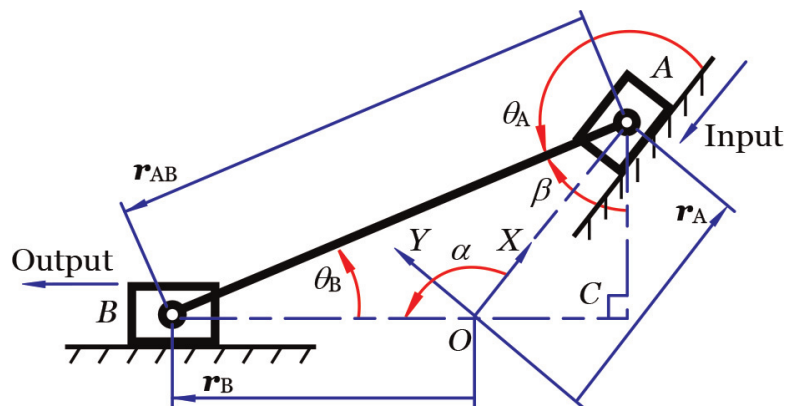

Figure 1.
Double-slider linkage.

Considering the symmetry, the case of $\alpha > 180°$ can be treated as the case of $\alpha < 180°$. Therefore, α is set to satisfy the following condition:

$$0 < \alpha < 180° \tag{3}$$

The solution of Eq. (2) for r_B with eliminating θ_A yields

$$r_B = \sqrt{r_{AB}^2 - r_A^2 \sin^2\alpha} + r_A \cos\alpha \tag{4}$$

$$\text{or } r_B = -\sqrt{r_A^2 - r_A^2 \sin^2\alpha} + r_A \cos\alpha \tag{5}$$

where Eq. (5) exists when the output slider is located at the right side of point C and moves right. With considering the symmetry, here we only discuss the case that the output slider is located at the left side of point C and moves left, which is described by Eq. (4).

The initial distance between origin O and point B corresponding to Eq. (4) is

$$r_{B0} = \sqrt{r_{AB}^2 - r_{A0}^2 \sin^2\alpha} + r_{A0} \cos\alpha \tag{6}$$

According to Eq. (4), we can further obtain

$$\frac{dr_B}{dr_A} = -\frac{r_A \sin^2\alpha}{\sqrt{r_{AB}^2 - r_A^2 \sin^2\alpha}} + \cos\alpha \tag{7}$$

Eq. (7) shows that if

$$r_A = r_{AB}/\tan\alpha \tag{8}$$

then

$$\frac{dr_B}{dr_A} = 0 \tag{9}$$

It indicates that if $AB \perp OA$, then the linkage is in kinematic limb-singularity which occurs when the instant velocity ratio between the output and the input is equal to zero.

If $r_A = \pm r_{AB}/\sin\alpha$, which occurs when $AB \perp OB$, then

$$\frac{dr_B}{dr_A} = \infty \tag{10}$$

It shows that the instant velocity ratio between the output and the input is equal to infinity, which is the kinematic actuation-singularity. Here we are limited to use the kinematic limb-singularity to design a mechanism with nonlinear stiffness by placing appropriate springs at corresponding joints. Therefore, the coordinate of the input slider should satisfy the kinematic constraint as follows:

$$-r_{AB}/\sin\alpha < r_A < r_{AB}/\sin\alpha \tag{11}$$

In order to pass the kinematic limb-singularity position, the initial coordinate/position of the input slider, r_{A0}, should satisfy

$$r_{A0} > r_{AB}/\tan\alpha \tag{12}$$

3. Force equilibrium equation

We suppose that each of the two prismatic joints is attached a translational spring and each of the two rotational joints is attached a torsional spring. The planar double-slider linkage with springs is obtained as shown in **Figure 2**. The stiffnesses of the translational springs placed at prismatic joints A and B are defined by k_{PA} and k_{PB}, respectively, and the stiffnesses of the translational springs placed at prismatic joints A and B are defined by k_{PA} and k_{PB}, respectively.

The potential energy of the whole mechanism as shown in **Figure 2** can be derived as

$$U = \frac{1}{2}k_{PA}(r_A - r_{A0})^2 + \frac{1}{2}(k_{RA} + k_{RB})(\theta_A - \theta_{A0})^2 + \frac{1}{2}k_{PB}(r_B - r_{B0})^2 \tag{13}$$

where θ_{A0} is the initial angle between positive direction of X-axis and coupler AB. After differentiating θ_A, θ_{A0}, r_B and r_{B0}, which can be derived from the geometry of the linkage as shown in **Figure 1**, with respect to r_A, and substituting them into Eq. (13), the following can be further derived:

$$U = \frac{1}{2}k_{PA}(r_A - r_{A0})^2 + \frac{1}{2}(k_{RA} + k_{RB})\left(\arccos\frac{r_A \sin\alpha}{r_{AB}} - \arccos\frac{r_{A0} \sin\alpha}{r_{AB}}\right)^2$$
$$+ \frac{1}{2}k_{PB}\left(\sqrt{r_{AB}^2 - r_A^2 \sin^2\alpha} + r_A \cos\alpha - \sqrt{r_{AB}^2 - r_{A0}^2 \sin^2\alpha} - r_{A0} \cos\alpha\right)^2. \tag{14}$$

The principle of virtual work, which does not need to determine the inner forces between two connected links, is a simplified useful method to construct the force equilibrium equation. According to the principle of virtual work, the required driving force, F_d, applied on the input slider can be obtained as

$$F_d = \frac{dU}{dr_A} = -k_{PA}(r_A - r_{A0}) + (k_{RA} + k_{RB})\left(\arccos\frac{r_A \sin\alpha}{r_{AB}} - \arccos\frac{r_{A0} \sin\alpha}{r_{AB}}\right)\frac{\sin\alpha}{\sqrt{r_{AB}^2 - r_A^2 \sin^2\alpha}}$$
$$+ k_{PB}\left(\sqrt{r_{AB}^2 - r_A^2 \sin^2\alpha} + r_A \cos\alpha - \sqrt{r_{AB}^2 - r_{A0}^2 \sin^2\alpha} - r_{A0} \cos\alpha\right)\left(\frac{r_A \sin^2\alpha}{\sqrt{r_{AB}^2 - r_A^2 \sin^2\alpha}} - \cos\alpha\right). \tag{15}$$

Here the input slider displacement is denoted by S, which satisfies

$$S = -r_A + r_{A0} \geq 0 \tag{16}$$

where $S \geq 0$ means the input slider moves along the negative direction of X-axis.
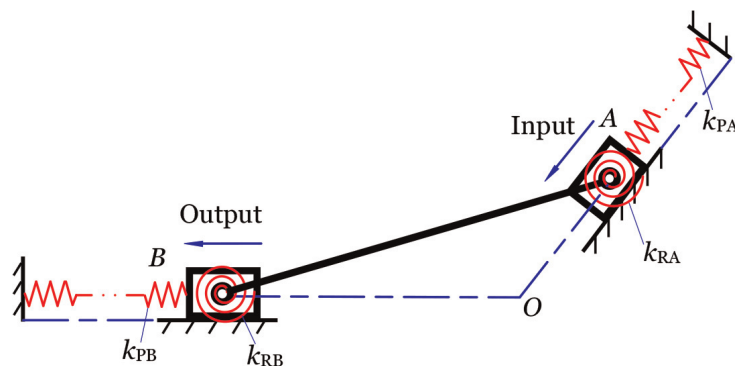

Figure 2.
Planar double-slider linkage with springs.

Substituting Eq. (16) into Eqs. (14) and (15), the potential energy, U, and the driving force, F_d, with respect to S can be obtained as

$$U = \frac{1}{2}k_{PA}S^2 + \frac{1}{2}(k_{RA} + k_{RB})\left(\arccos\frac{(r_{A0} - S)\sin\alpha}{r_{AB}} - \arccos\frac{r_{A0}\sin\alpha}{r_{AB}}\right)^2$$

$$+ \frac{1}{2}k_{PB}\left(\sqrt{r_{AB}^2 - (r_{A0} - S)^2\sin^2\alpha} + (r_{A0} - S)\cos\alpha - \sqrt{r_{AB}^2 - r_{A0}^2\sin^2\alpha} - r_{A0}\cos\alpha\right)^2.$$

$$\tag{17}$$

$$F_d = \frac{dU}{dS} = k_{PA}S + (k_{RA} + k_{RB})\left(\arccos\frac{(r_{A0} - S)\sin\alpha}{r_{AB}} - \arccos\frac{r_{A0}\sin\alpha}{r_{AB}}\right)\frac{\sin\alpha}{\sqrt{r_{AB}^2 - (r_{A0} - S)^2\sin^2\alpha}}$$

$$+ k_{PB}\left((r_{A0} - S)\cos\alpha + \sqrt{r_{AB}^2 - (r_{A0} - S)^2\sin^2\alpha} - r_{A0}\cos\alpha - \sqrt{r_{AB}^2 - r_{A0}^2\sin^2\alpha}\right)$$

$$\times \left(\frac{(r_{A0} - S)\sin^2\alpha}{\sqrt{r_{AB}^2 - (r_{A0} - S)^2\sin^2\alpha}} - \cos\alpha\right).$$

$$\tag{18}$$

From Eq. (18), we can predict that the variation of driving force exerted on the input slider versus input displacement, i.e., F_d-S curve, would present nonlinear stiffness characteristic.

4. Cause of nonlinear stiffness characteristic generation

It is evident that the springs placed at joints are the cause of nonlinear stiffness characteristic generation, so it is necessary to discuss the influence of spring stiffness on the F_d-S curve characteristic. When the influence of one specific spring stiffness is analysed, every other spring stiffness is set to zero.

4.1 Influences of translational spring stiffness placed at output slider

Substituting k_{PA} = 0 and k_{RA} = k_{RB} = 0 into Eqs. (17) and (18), the following can be obtained, respectively:

$$U = \frac{1}{2}k_{PB}\left((r_{A0} - S)\cos\alpha + \sqrt{r_{AB}^2 - (r_{A0} - S)^2\sin^2\alpha} - r_{A0}\cos\alpha - \sqrt{r_{AB}^2 - r_{A0}^2\sin^2\alpha}\right)^2$$

$$\tag{19}$$

$$F_d = \frac{dU}{dS} = k_{PB}\left((r_{A0} - S)\cos\alpha + \sqrt{r_{AB}^2 - (r_{A0} - S)^2\sin^2\alpha} - r_{A0}\cos\alpha - \sqrt{r_{AB}^2 - r_{A0}^2\sin^2\alpha}\right)$$

$$\times \left(\frac{(r_{A0} - S)\sin^2\alpha}{\sqrt{L^2 - (r_{A0} - S)^2\sin^2\alpha}} - \cos\alpha\right).$$

$$\tag{20}$$

When Eq. (20) is zero, solving this equation with respect to S obtains

$$S_1 = 0, \quad S_2 = -r_{AB}/\tan\alpha + r_{A0}, \quad S_3 = -2r_{A0}\cos^2\alpha - 2\sqrt{r_{AB}^2 - r_{A0}^2\sin^2\alpha}\cos\alpha + 2r_{A0}$$

(21)

where S_2 is the kinematic limb-singularity position (based on Eqs. (8) and (16)). From Eq. (19), we know that

$$U|_{S=S_1} = U|_{S=S_3} = 0$$

(22)

Substitution of Eq. (16) into the differentiation of Eq. (20) with respect to S leads to

$$\left.\frac{dF_d}{dS}\right|_{S=S_2} = \left.\frac{d^2U}{dS^2}\right|_{S=S_2} = -k_{PB}\left(\frac{r_{AB}}{\sin\alpha} - r_{B0}\right) \cdot \frac{1}{r_{AB}\sin\alpha} < 0.$$

(23)
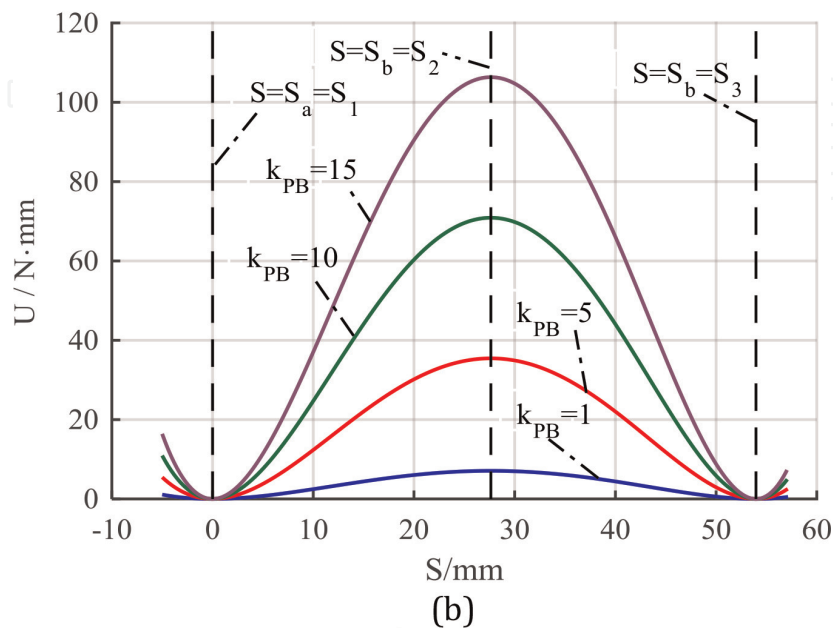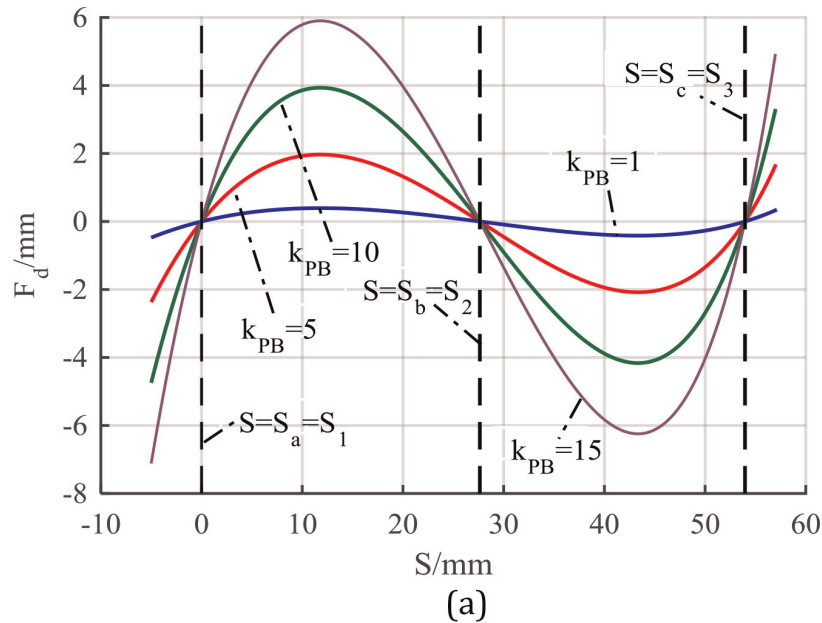
Figure 3.
The bistable characteristic with different k_{PB} when $k_{PA} = k_{RA} = 0$ and $k_{RB} = 0$. (a) Driving force versus input displacement. (b) Potential energy versus input displacement.

Eq. (23) shows that when $S = S_2$, the potential energy, U, reaches the local maximum. Therefore, $S = S_2$, the kinematic limb-singularity position, is also the unstable equilibrium position [15].

Therefore, according to [15], when $k_{PA} = 0$, $k_{RA} = k_{RB} = 0$ and $k_{PB} \neq 0$, the kinematic limb-singularity position, S_2, is the mechanism's unstable equilibrium position and S_1 and S_3 are the stable equilibrium points.

If the coupler length, r_{AB}, is 100 mm; intersection angle, α, is 100°; initial input slider position, r_{A0}, is 10 mm; and the unit of k_{PB} is N/mm (here the unit of translational spring stiffness is N/mm, and the unit of torsional spring stiffness is N·mm/rad); the stiffness characteristic produced by the mechanism is shown in **Figure 3**.

Figure 3 confirms that when the spring stiffness placed at output slider is exclusively zero, the mechanism produces the bistable characteristic.

4.2 Influences of translational spring stiffness placed at input slider

Substitution of $k_{PB} = 0$ and $k_{RA} = k_{RB} = 0$ into Eqs. (17) and (18) obtains the expressions as follows:

$$U = \frac{1}{2}k_{PA}S^2 \qquad (24)$$

$$F_d = k_{PA}\,S \qquad (25)$$
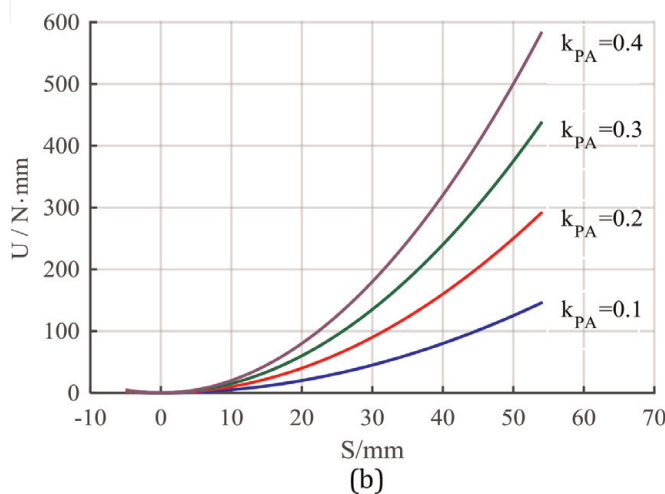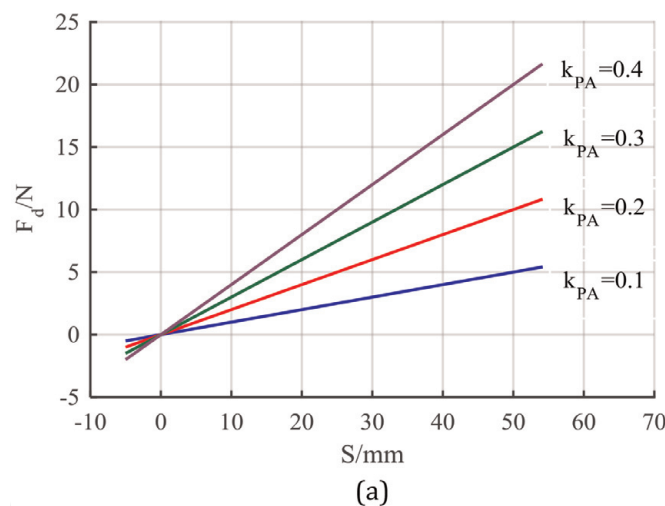
Figure 4.
Stiffness characteristic with different k_{PA} *when* $k_{RA} = k_{RB} = k_{PB} = 0$. *(a) Driving force versus input displacement. (b) Potential energy versus input displacement.*

Eqs. (24) and (25) show that the mechanism only generates positive-stiffness characteristic when the mechanism has only one minimal potential energy point, which can be confirmed by **Figure 4**, where specific parameters are given as $r_{AB} = 100$ mm, $\alpha = 100°$ and $r_{A0} = 10$ mm.

4.3 Influences of torsional spring stiffness placed at pin joints

When $k_{PA} = k_{PB} = 0$ and $k_{RA} = k_{RB} \neq 0$, from Eq. (18), we can obtain

$$F_d = (k_{RA} + k_{RB}) \left(\arccos \frac{(r_{A0} - S) \sin \alpha}{r_{AB}} - \arccos \frac{r_{A0} \sin \alpha}{r_{AB}} \right) \frac{\sin \alpha}{\sqrt{r_{AB}^2 - (r_{A0} - S)^2 \sin^2 \alpha}}$$

(26)

where only and only if $S = S_1 = 0$, i.e., $r_A = r_{A0}$, then $F_d = 0$.

In other words, if and only if $S = S_1 = 0$, the mechanism is in equilibrium position without external force. When the mechanism is located in any other positions, it is unstable except when applied by external force. Meanwhile, the potential energy, U, has no local maximum but has only one minimum which is located at $S = S_1 = 0$.

For $k_{PA} = k_{PB} = 0, k_{RA} = k_{RB} \neq 0$, when $r_{AB} = 100$ mm, $\alpha = 100°$ and $r_{A0} = 10$ mm, the force-displacement characteristic and the potential energy curve are shown in **Figure 5**.
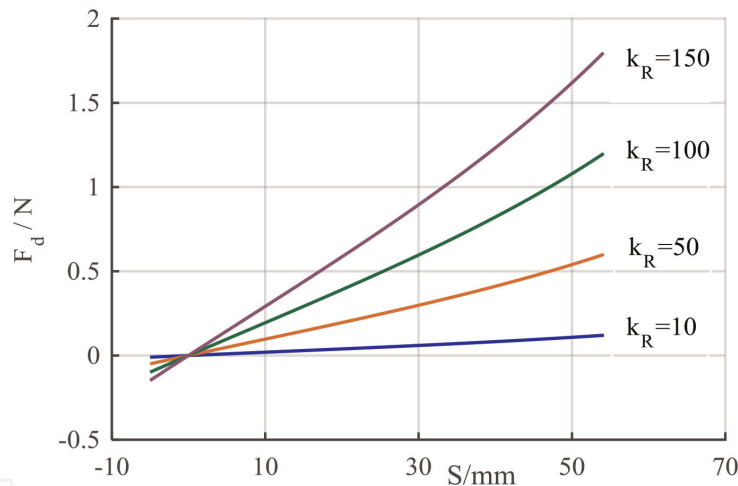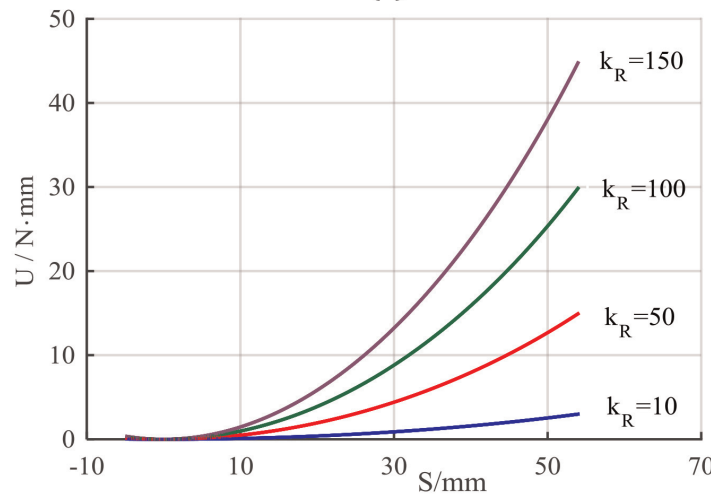

Figure 5.
Behaviours with different $k_{RA} = k_{RB} = k_R$ *when* $k_{PB} = 0$ *and* $k_{PA} = 0$. *(a) Driving force versus input displacement. (b) Potential energy versus input displacement.*

Figure 5 demonstrates that when the torsional springs are placed at the pin joints, the mechanism only produces positive-stiffness characteristic but does not produce other stiffness characteristic.

5. Nonlinear stiffness characteristic construction

Section 4 showed that spring placed at the output slider causes the bistable characteristic with the negative domain, while springs placed at other joints produce the corresponding positive-stiffness characteristic. It can be predicted that if more than one spring are placed at joints, when the mechanism moves from non-singular position (**Figure 6(a)**) to another non-singular position (**Figure 6(c)**) while passing through the limb-singularity position (**Figure 6(b)**), the stiffness characteristic of the mechanism is the superposition of the corresponding stiffness characteristic caused by the joints. For instance, if $k_{PB} = 1$ N/mm, $\alpha = 100°$,
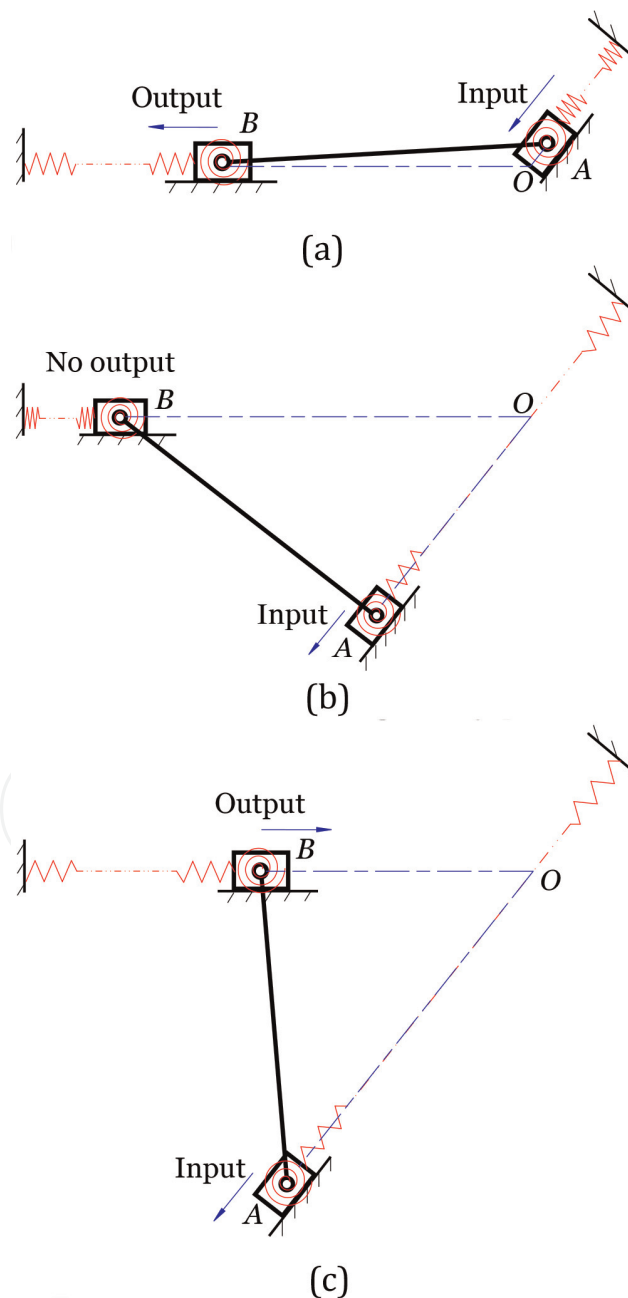

Figure 6.
Positions of the mechanism. (a) Initial kinematic non-singular position. (b) Kinematic limb-singularity position. (c) End kinematic non-singular position.

r_{A0} = 10 mm and r_{AB} = 100 mm, several nonlinear stiffness characteristics with different spring stiffness are shown in **Figure 7**.

Figure 7 shows that after assigning appropriate spring stiffness placed at the corresponding joints, the mechanism can generate one of four types of nonlinear
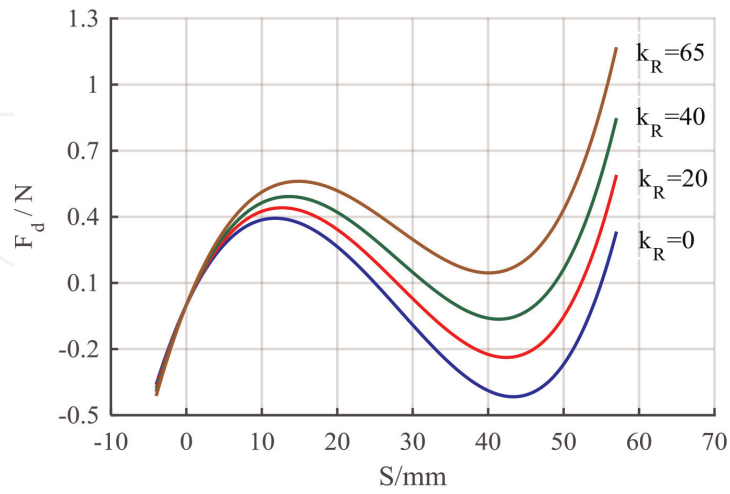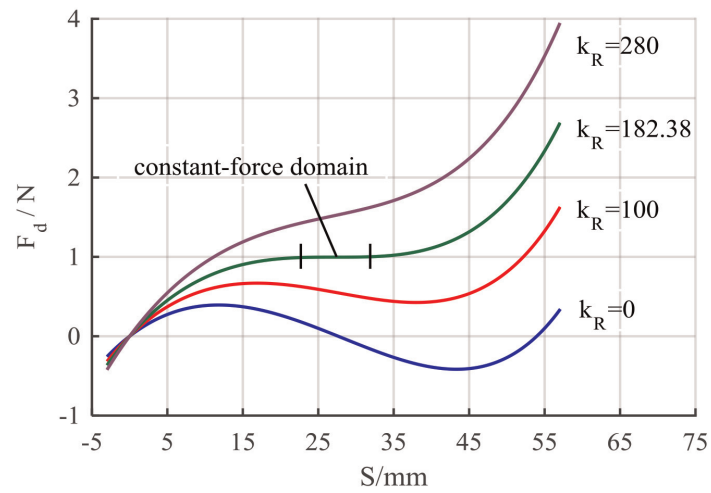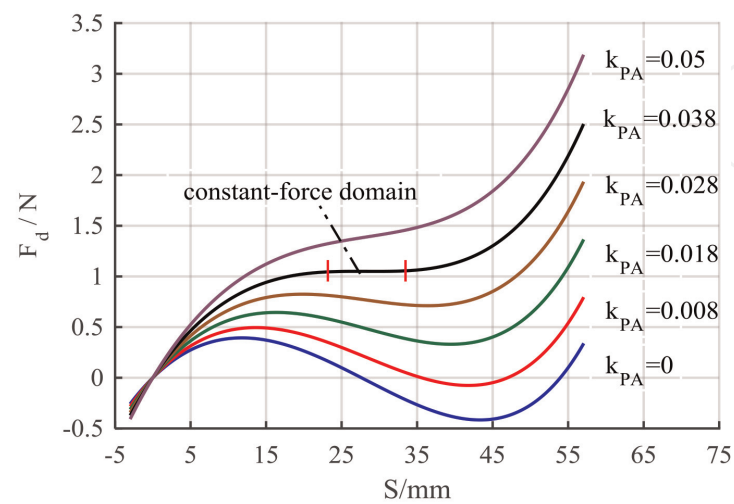
Figure 7.
Nonlinear stiffness characteristic when k_{PB} = 1 N/mm. (a) Driving force versus input displacement for minor change of $k_{RA} = k_{RB} = k_R$ when k_{PA} = 0. (b) Driving force versus input displacement for large change of $k_{RA} = k_{RB} = k_R$ when k_{PA} = 0. (c) Driving force versus input displacement for different spring stiffness when $k_{RA} = k_{RB} = 0$.
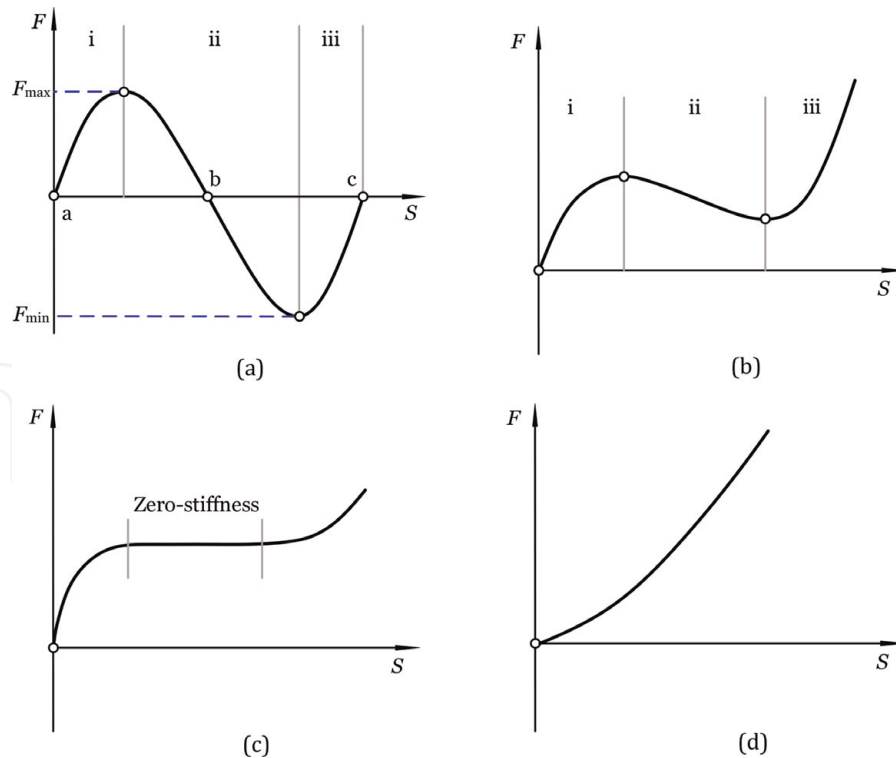
Figure 8.
Four types of nonlinear stiffness characteristic of the mechanism. (a) Bistable characteristic, (b) partial negative-stiffness characteristic, (c) partial zero-stiffness characteristic, and (d) positive-stiffness characteristic.

stiffness characteristics including bistable characteristic, partial negative-stiffness characteristic, partial zero-stiffness characteristic and positive-stiffness characteristic which are shown in **Figure 8**, as it works around the kinematic limb-singularity position.

The above-mentioned analysis illustrates the case that the mechanism moves from a non-singular position. When the mechanism moves from the kinematic limb-singularity position (**Figure 6(b)**) to a non-singular position (**Figure 6(c)**), every spring transforms with zero potential energy to a position with a certain amount of potential energy. The total potential energy of the mechanism starts from zero to nonzero without local minimal energy point except the initial position. Every spring force/torque increases in the process of the mechanism's motion. From Eqs. (18) or (20), the driving force is to overcome the resistance caused by every spring, so the driving force increases when the mechanism moves from non-singular position. In other words, when mechanism moves from non-singular position with no deflected springs, the mechanism only generates the positive-stiffness characteristic as shown in **Figure 8(d)**. If $k_{PA} = k_{PB} = 0$, $k_{RA} = k_{RB} \neq 0$ and $r_{AB} = 100$ mm, $\alpha = 100°$ and $r_{A0} = 10$ mm, the stiffness characteristic is shown in **Figure 9**.

Figure 9 demonstrates that when the mechanism starts from the kinematic limb-singularity position with no deflected springs towards a non-singular position, it only generates positive-stiffness characteristic.

As the final stiffness characteristic is determined by the superposition of stiffness characteristic caused by each spring, an expected stiffness characteristic can be constructed by assigning appropriate values to k_{PB}, k_{RA}, k_{RB} and k_{PA} on the condition of $k_{RB} \neq 0$ when the mechanism moves from one non-singular position to another non-singular position with passing through the kinematic limb-singularity position. The method for designing an expected nonlinear stiffness design is proposed in [16].
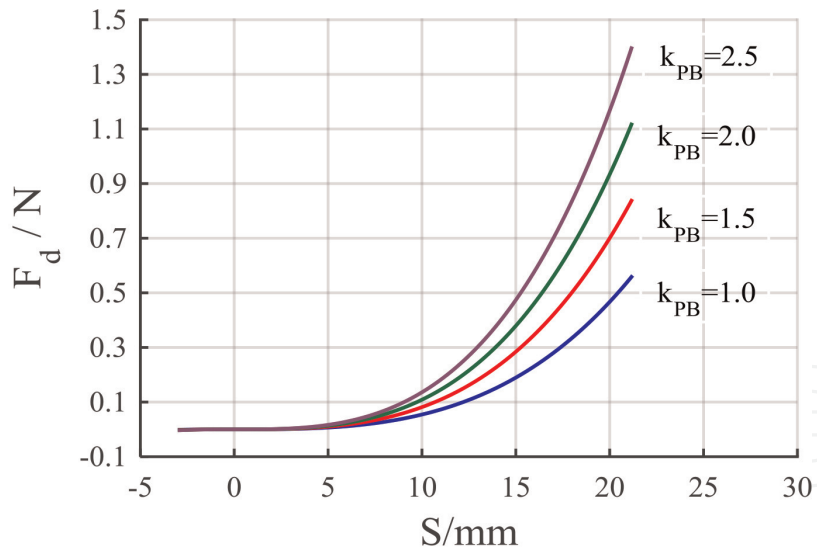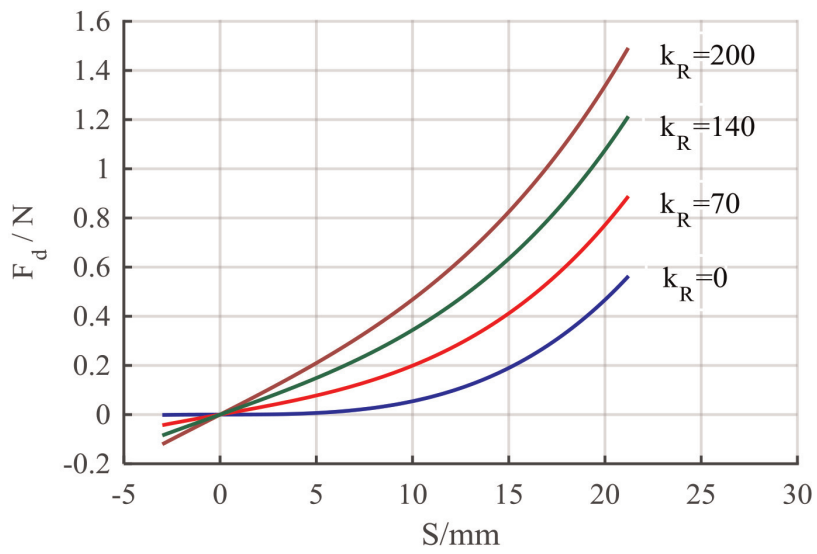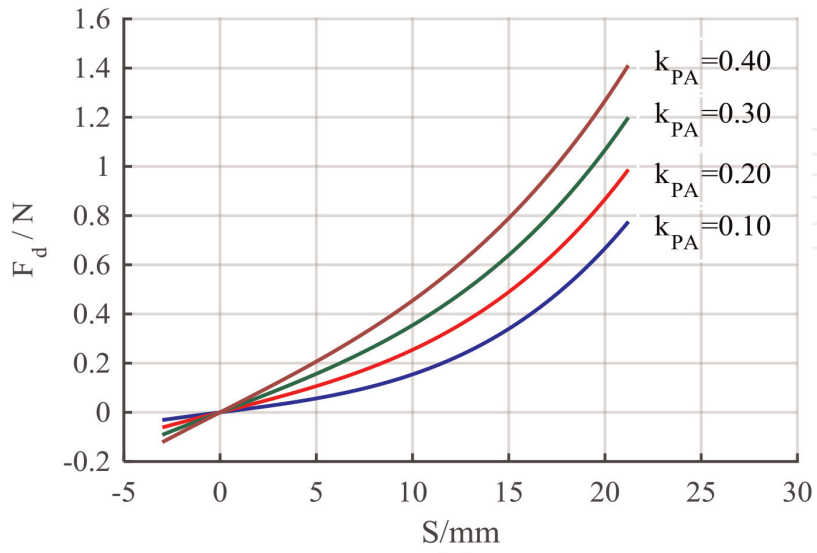
Figure 9.
Stiffness characteristic with initial non-singular position. (a) Stiffness characteristic for different k_{PB} when $k_{RA} = k_{RB} = 0$ and $k_{PA} = 0$. (b) Stiffness characteristic for different $k_{RA} = k_{RB} = k_R$ when $k_{PB} = 1$ N/mm and $k_{PA} = 0$. (c) Stiffness characteristic for k_{PA} when $k_{PB} = 1$ N/mm and $k_{RA} = k_{RB} = 0$.

6. Further discussion

From Sections 2–5, it can be shown that if a planar linkage exhibits a kinematic limb-singularity, it generates different nonlinear spring stiffness characteristics if the linkage is added with springs at corresponding joints with the condition that the spring stiffness corresponding to output slider is nonzero. Nonlinear stiffness characteristic generation using the kinematic limb-singularity of a planar linkage can be demonstrated by another planar linkage with springs as shown in **Figure 10**, which represents a crank-slider linkage with springs.

The Cartesian coordinates system, O-xyz, is constructed as shown in **Figure 10**, where crank AB rotates about joint A in an anticlockwise direction, the slider moves along the x-axis, and coupler BC connects link AB and slider by two rotation joints B and C. The three rotation joints are added with torsional springs with spring stiffnesses denoted by K_{RA}, K_{RB} and K_{RC}, respectively. An extension spring is placed at the output slider and its stiffness is denoted by K_{PC}.

The position formula with closed-loop form, whose derivation process is similar to one of the double-slider four-bar linkages, can be established easily (not shown here).

Based on the position analysis, the kinetostatic model of the mechanism by using the principle of virtual work can be constructed as

$$
T_\mathrm{d} = K_\mathrm{RA}(\theta_\mathrm{A} - \theta_\mathrm{A0}) + K_\mathrm{RB}\left(-\theta_\mathrm{A} - \arcsin\frac{r_1 \sin\theta_\mathrm{A} - e}{r_2} + \theta_\mathrm{A0} + \arcsin\frac{r_1 \sin\theta_\mathrm{A0} - e}{r_2}\right)
$$

$$
\times(-1 - r_1\cos\theta_\mathrm{A}/a)
$$

$$
+ K_\mathrm{RC}\left(\arcsin\frac{r_1 \sin\theta_\mathrm{A} - e}{r_2} - \arcsin\frac{r_1 \sin\theta_\mathrm{A0} - e}{r_2}\right) \times \frac{r_1\cos\theta_\mathrm{A}}{a}
$$

$$
+ K_\mathrm{PC}(r_1\cos\theta_\mathrm{A} + a - r_1\cos\theta_\mathrm{A0} - a_0) \times (-r_1\sin\theta_\mathrm{A} - b/a)
$$

$$
\tag{27}
$$

where r_1 and r_2 are crank length and coupler length, respectively, r_3 is the X-axis coordinate of output slider and e is the offset.

Moreover, a and a_0 are defined by

$$
a = \sqrt{r_2^2 - (r_1\sin\theta_\mathrm{A} - e)^2}, a_0 = \sqrt{r_2^2 - (r_1\sin\theta_\mathrm{A0} - e)^2}
$$

According to Eq. (27), the T_d-θ_A (driving torque versus input position angle) curve can be described.
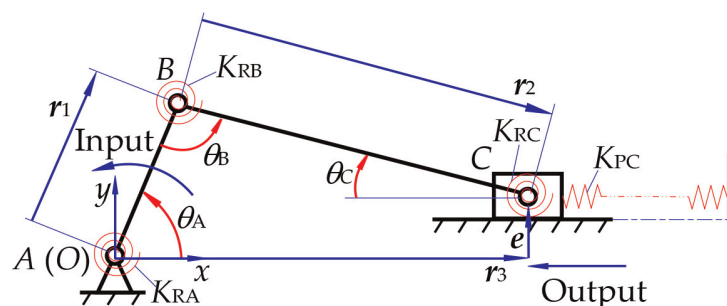

Figure 10.
Crank-slider with springs.
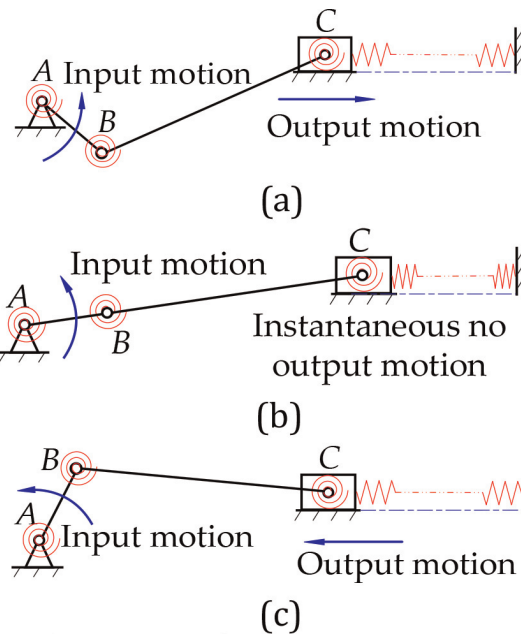
Figure 11.
Different positions of the crank-slider mechanism with springs. (a) Non-singular initial position. (b) Kinematic limb-singularity position. (c) Non-singular end position.
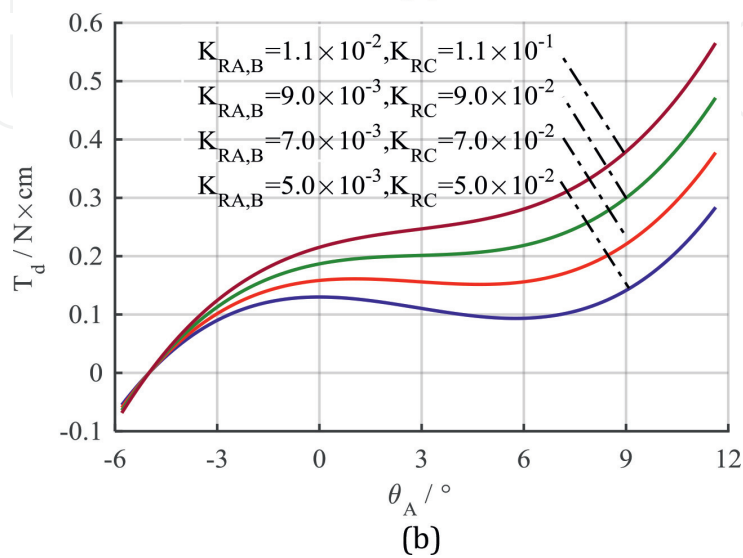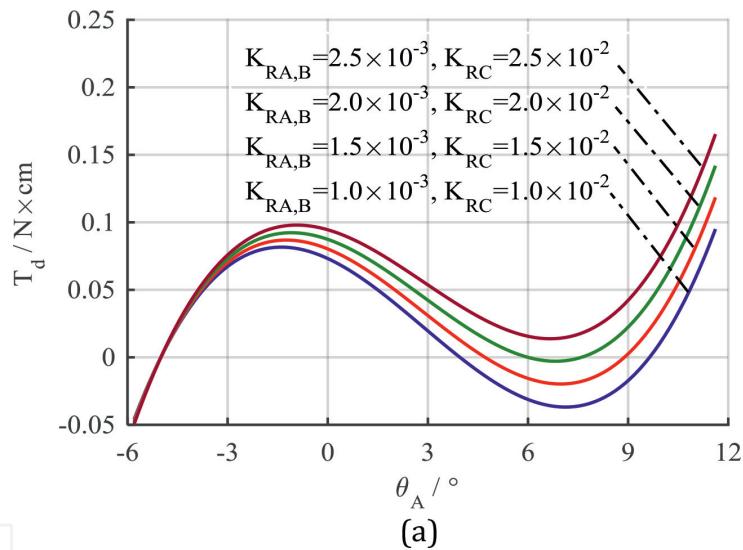

Figure 12.
Case that the mechanism moves from non-singular position. (a) Input torque variation when $K_{RA} = K_{RB} = K_R$ is small. (b) Input torque variation when $K_{RA} = K_{RB} = K_R$ is large.
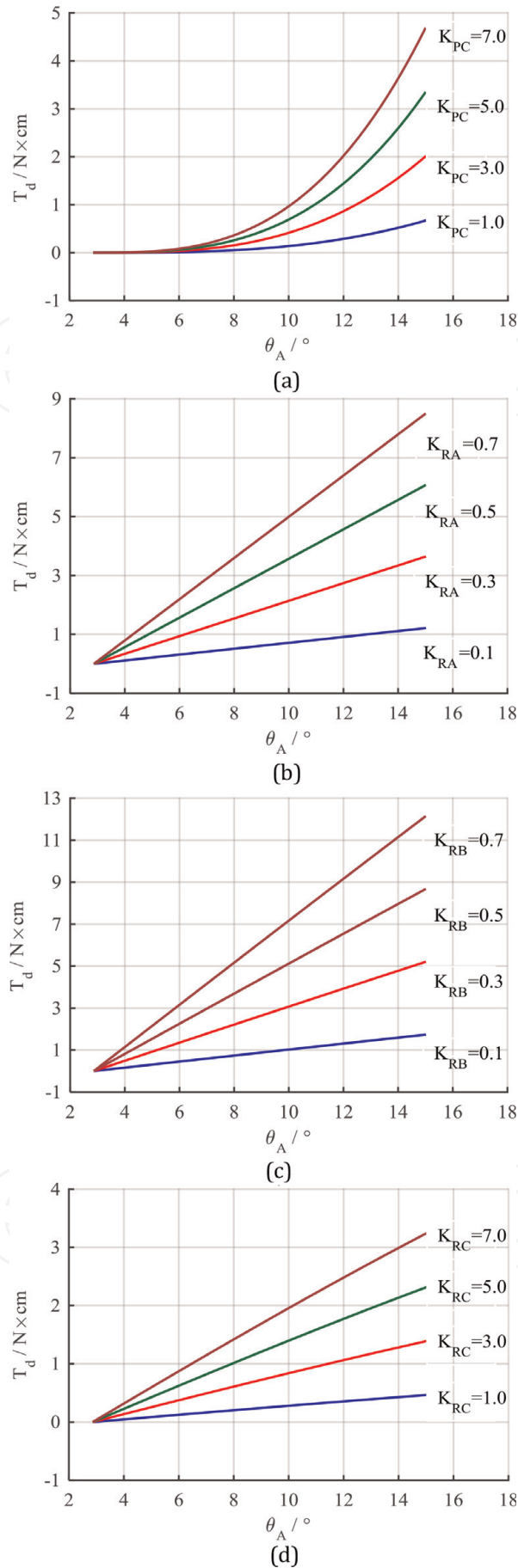
Figure 13.
Case that the mechanism moves from kinematic limb-singularity position. (a) Case of different K_{PC} when $K_{RA} = K_{RB} = K_{RC} = 0$. (b) Case of different K_{RA} when $K_{RB} = K_{RC} = 0$ and $K_{PC} = 0$. (c) Case of different K_{RB} when $K_{RA} = K_{RC} = 0$ and $K_{PC} = 0$. (d) Case of different K_{RC} when $K_{RA} = K_{RB} = 0$ and $K_{PC} = 0$.
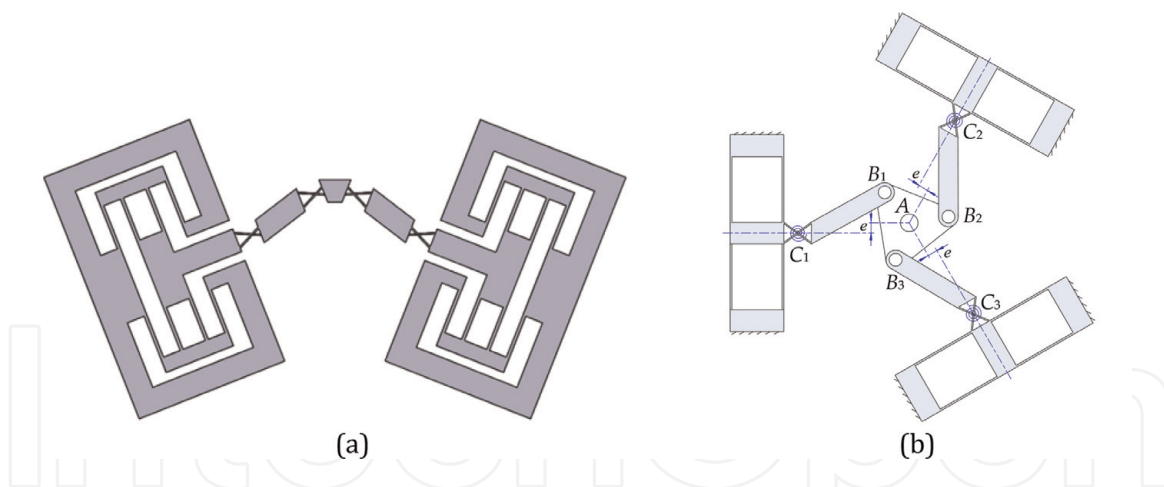
Figure 14.
Nonlinear stiffness characteristic compliant mechanisms based on the PRBM. (a) Compliant double-slider mechanism and (b) compliant crank-slider mechanism.

When the mechanism with springs moves from one non-singular position to the kinematic limb-singularity position and then stops at another non-singular position as shown in **Figure 11**, it may produce one of four types of nonlinear stiffness characteristics including the bistable characteristic, partial negative-stiffness characteristic, partial zero-stiffness characteristic and positive-stiffness characteristic. For illustration, in **Figure 12**, crank length, r_1, is 10 cm; coupler length, r_2, is 50 cm; offset e is 3 cm; input initial position angle, θ_{A0}, is $-5°$; and K_{PC} = 1 N/cm.

It can also be shown that, similarly to the double-slider four-bar mechanism with springs, when the crank-slider mechanism with springs moves from the kinematic limb-singularity position, it only generates the positive-stiffness characteristic, which is shown in **Figure 13**, where the geometry parameters are given as the same as shown in **Figure 12**.

Therefore, we can conclude that after placing springs at different pair combinations, a planar linkage which has the kinematic limb-singularity can generate corresponding nonlinear stiffness characteristic in condition that the mechanism moves from initial non-singular position with no deflected springs to the kinematic limb-singularity position and then stops at another non-singular position. If the mechanism moves from the kinematic limb-singularity position with no deflected springs, it only generates the positive-stiffness characteristic.

It is worth to point out that the nonlinear stiffness characteristic generation method can also be applied to design the nonlinear stiffness characteristic compliant mechanism by using the PRBM as shown in **Figure 14**.

In **Figure 14**, the equivalent stiffness of compliant rotational joint and compliant translational joint can be calculated by referring to previous work [17, 18].

7. Conclusions

The kinematic limb-singularity positions of planar linkages with attached springs can be used to generate nonlinear characteristics. After assigning different spring stiffness, the mechanism may exhibit one of four types of nonlinear stiffness characteristics. These are the bistable characteristic, partial negative-stiffness characteristic, partial zero-stiffness characteristic and positive-stiffness characteristic. The type of stiffness characteristic is determined by the motion model and the value of spring stiffness. On the condition that the mechanism moves from the initial non-singular position to another non-singular position with passing though the

kinematic limb-singularity position, spring stiffness determines one of four types of stiffness characteristics. On the other hand, when the mechanism moves from the kinematic limb-singularity position, it only produces the positive-stiffness characteristic.

Acknowledgements

Author details

Baokun Li[1] and Guangbo Hao[2]*

1 School of Mechanical Engineering, Anhui University of Science and Technology, Huainan, China

2 School of Engineering, University College Cork, Cork, Ireland

*Address all correspondence to: g.hao@ucc.ie

IntechOpen

References

[1] Huang Z, Zhao YS, Zhao TS. Advanced Spatial Mechanism. Beijing, China: Higher Education Press; 2005. (in Chinese)

[2] Gosselin CM, Angeles J. Singularity analysis of closed loop kinematic chains. IEEE Transactions on Robotics and Automation. 1990;**6**(3):281-290. DOI: 10.1109/70.56660

[3] Amine S, Mokhiamar O, Caro S. Classification of 3T1R parallel manipulators based on their wrench graph. ASME Journal of Mechanisms and Robotics. 2017;**9**(1):011003. DOI: 10.1115/1.4035188

[4] Huang Z, Cao Y. Property identification of the singularity loci of a class of Gough-Stewart manipulators. The International Journal of Advanced Robotics Research. 2005;**24**(8):375-685. DOI: 10.1177/0278364905054655

[5] Boudreau R, Nokleby S. Force optimization of kinematically-redundant planar parallel manipulators following a desired trajectory. Mechanism and Machine Theory. 2012; **56**(10):138-155. DOI: 10.1016/j. mechmachtheory.2012.06.001

[6] Saglia J, Dai JS, Caldwell DG. Geometry and kinematic analysis of a redundantly actuated parallel mechanism that eliminates singularity and improves dexterity. ASME Journal of Mechanical Design. 2008;**130**(12): 124501. DOI: 10.1115/1.2988472

[7] Li B, Cao Y, Zhang Qiuju, et al. Position-singularity analysis of a special class of the Stewart parallel mechanisms with two dissimilar semi-symmetrical hexagons. Robotica. 2013;**31**(1):123-136. DOI: 10.1017/S0263574712000148

[8] Karimia A, Masouleha MT, Cardoub P. Avoiding the singularities of 3-RPR parallel mechanisms via dimensional

synthesis and self-reconfigurability. Mechanism and Machine Theory. 2016; **99**:189-206. DOI: 10.1016/j. mechmachtheory.2016.01.006

[9] Abhilash N, Li H, Hao G, et al. A reconfigurable compliant four-bar mechanism with multiple operation modes. In: ASME International Design Engineering Technical Conferences & Computers and Information in Engineering Conference; August 6–9, 2017; Cleveland, Ohio, USA; DETC2017–67441; 2017. DOI: 10.1115/ DETC2017-67441

[10] Rubbert L, Caro S, Gangloff J, et al. Using singularities of parallel manipulators for enhancing the rigid-body replacement design method of compliant mechanisms. ASME Journal of Mechanical Design. 2014;**136**(5): 051010. DOI: 10.1115/1.4026949

[11] Rubbert L, Renaud P, Caro S, et al. Design of a compensation mechanism for an active cardiac stabilizer based on an assembly of planar compliant mechanisms. Mechanics and Industry. 2014;**15**(2):147-151. DOI: 10.1051/meca/ 2014013

[12] Quentin B, Marc V, Salih A. Parallel singularities for the design of softening springs using compliant mechanisms. In: ASME International Design Engineering Technical Conferences & Computers and Information in Engineering Conference; August 2–5, 2015; Boston, Massachusetts, USA; DETC2015-47240; 2015. DOI: 10.1115/DETC2015-47240

[13] Gallego JA, Herder J. Synthesis methods in compliant mechanisms: An overview. In: ASME International Design Engineering Technical Conferences and Computers and Information in Engineering Conference & Computers and Information in Engineering Conference; August

30–September 2, 2009; San Diego, California, USA; DETC2009–86845; 2009. DOI: 10.1115/DETC2009-86845

[14] Olsen BM, Issac Y, Howell LL, et al. Utilizing a classification scheme to facilitate rigid-body replacement for compliant mechanism design. In: ASME International Design Engineering Technical Conferences & Computers and Information in Engineering Conference; August 15–18, 2010; Montreal, Quebec, Canada; DETC2010–28473; 2010. DOI: 10.1115/DETC2010-28473

[15] Baker MS, Howell LL. On-chip actuation of an in-plane compliant bistable micromechanism. Journal of Microelectromechanical Systems. 2002; **11**(5):566-573. DOI: 10.1109/JMEMS.2002.803284

[16] Li B, Hao G. Nonlinear behaviour design using the kinematic singularity of a general type of double-slider four-bar linkage. Mechanism and Machine Theory. 2018;**129**:106-130. DOI: 10.1016/j.mechmachtheory.2018.07.016

[17] Zhao H, Bi S, Yu J. Nonlinear deformation behavior of a beam-based flexural pivot with monolithic arrangement. Precision Engineering. 2011;**35**(2):369-382. DOI: 10.1016/j.precisioneng.2010.12.002

[18] Pei X, Yu J, Zong G, et al. The modeling of cartwheel flexural hinges. Mechanism and Machine Theory. 2009; **44**(10):1900-1909. DOI: 10.1016/j.mechmachtheory.2009.04.006